Computational Materials Science 95 (2014) 256–262

Contents lists available at ScienceDirect

Computational Materials Science

journal homepage: www.elsevier.com/locate/commatsci

An efficient method to generate amorphous structures based on local geometry

Yong Youn, Youngho Kang, Seungwu Han *

Department of Materials Science and Engineering and Research Institute of Advanced Materials, Seoul National University, Seoul 151-744, Republic of Korea

ARTICLE INFO

Article history:
Received 20 May 2014
Received in revised form 26 July 2014
Accepted 30 July 2014

Keywords:
Amorphous structure modeling
Seed-coordinate-anneal
Ab initio method

ABSTRACT

We propose an efficient method that generates amorphous structures based on information on the short-range order such as bond lengths and coordination numbers. The base amorphous structure is constructed in the "seed-and-coordinate" style, which conforms to the given short-range order. The structure is further annealed to relax the atomic bonding and establish the medium-range order. The computational cost of the proposed method is less than 10% of the standard melt-quench approach. We combine this method with *ab initio* calculations and generate amorphous structures for various materials such as *a*-Si, *a*-SiO_2, *a*-$Ge_2Sb_2Te_5$, and *a*-$InGaZnO_4$. The obtained structures are close to those from melt-quench simulations in terms of atomic and electronic structures. To substantiate the computational efficiency, we generate *a*-GeSe with 512 atoms in the unit cell. The large cell allows us for identifying the mobility edge clearly.

1. Introduction

In many applications, crystalline materials are usually favored owing to good stability and well-defined physical properties. Nevertheless, the metastability or non-equilibrium state of amorphous structures also leads to useful applications. For example, the structural flexibility of amorphous SiO_2 (*a*-SiO_2) has been used for shaping glasses in various forms since long time ago. More recently, the hydrogenated amorphous Si (*a*-Si:H) has been widely used in electronic devices that require a large-area growth of electrically active materials [1,2]. Furthermore, *a*-Si is now challenged by another amorphous material, In–Ga–Zn–O, which shows larger electron mobilities [3–8] Lastly, the phase-change memory that exploits reversible switching between amorphous and crystalline phases of chalcogenides such as $Ge_2Sb_2Te_5$, is a leading contender for the next-generation nonvolatile memory [9–12].

The conventional spectroscopic analysis is seriously limited when studying amorphous materials due to the lack of lattice periodicity. This made the computational modeling on amorphous phases very informative because it can provide structural and electronic data that are not accessible in experiment. However, in contrast to the crystalline phase, detailed atomic arrangements in amorphous materials are not available prior to the simulation. This is a serious hurdle against the atomistic simulation, in which the knowledge on atomic positions is a prerequisite. So far, several methods have been developed to generate amorphous structures theoretically [13,14]. One example is the bond-switching method [15], which was successfully applied to generate the continuous random network (CRN) structures for sp^3 semiconductors like *a*-Si, *a*-Ge, and amorphous diamond. However, this method is rather limited to CRN structures with strong covalent characters. In addition, the ideal CRN model is sometimes inconsistent with experiment [16]. Activation-relaxation technique (ART) is another well-established approach [17–20]. In this case, the atomic positions are activated from the local energy minimum to an adjacent saddle point and then relaxed to another local minimum following the downhill paths in the energy landscape.

Perhaps, the most favored method at present is the melt-quench (MQ) approach based on molecular dynamics (MD) simulation. This mimics the actual MQ process in experiment. If a reliable force field or interatomic potential is available, the classical MD simulation will be able to produce amorphous structures very efficiently [21–24]. However, the classical force field is highly limited in the choice of material classes. Such a limitation does not exist in the *ab initio* MD simulation based on the density functional theory (DFT) in which the atomic forces are obtained through quantum-mechanical description of electronic states. Therefore, the MQ method based on DFT-MD has been applied to generating amorphous structures of a wide range of materials in a reliable way [25–33]. However, the computational cost of DFT-MD is so expensive that supercells comprise only about 100–200 atoms in most

* Corresponding author.
E-mail address: hansw@snu.ac.kr (S. Han).

http://dx.doi.org/10.1016/j.commatsci.2014.07.053
0927-0256/

cases. With a typical size of modern computational clusters, it takes weeks of computational time to obtain one amorphous structure including 100–200 atoms in the unit cell. If one employs a relatively big supercell with >500 atoms [34] or generates multiple amorphous structures for statistical average [35], the computational time easily scales up to several months.

In this work, we propose a new computational scheme to produce the amorphous structure, which utilizes DFT but is faster than the conventional DFT-based MQ method by more than ten folds. Our method starts with the premise that if the detailed information on the short-range order is available beforehand, one can quickly generate a reasonable amorphous model in one-shot and only short time annealing would be necessary to refine the structure. The reference local order could be obtained experimentally through the reverse Monte Carlo method [36,37] or theoretically from the MQ amorphous structure. In the latter case, we note that the short-range order is well addressed in relatively small supercells consisting of less than 100 atoms. Therefore, the basic strategy of the present method is that one performs the MQ simulation on a small cell and extracts the detailed local order, which is used in generating amorphous structures on a large scale or multiple times for the statistical average, within a reasonable computational time.

The paper is organized as follows. In Section 2.1, we define various parameters required for generating the structure. The detailed algorithm (so called "seed-coordinate-anneal") is put forward in Section 2.2. Test calculations on various amorphous materials (Si, SiO_2, $Ge_2Sb_2Te_5$, and $InGaZnO_4$) are presented in Section 3 with comparison with reference structures and experiment. Finally, we summarize and conclude in Section 4.

2. Computational method

2.1. Input parameters defining the local geometry

In the following, we assume that the detailed information on the short-range order is available from either the reference calculations involving a small number of atoms or reverse Monte Carlo analysis on the experimental diffraction data. We then define variables specifying the local geometry of the reference structures. The basic bonding information is determined by the atom-resolved radial distribution function (RDF). For easy understanding, the procedure will be described with the specific example of *a*-GeSe as shown in Fig. 1. The topmost figures in Fig. 1(a) and (b) are partial RDFs around Ge and Se atoms with the first-dip position indicated by the dashed line. If the fully resolved RDF between *X* and *Y* (*X*, *Y* = Ge or Se) has the first peak within the dashed line, it is assumed that bonds are formed between *X* and *Y*. According to this criterion, bonds are not formed between Se atoms as the first peak in the bottom picture of Fig. 1(b) lies outside the dashed line. The bonding ranges for Ge–Ge, Ge–Se and Se–Ge pairs are parameterized by $d^X_{\min}(Y)$ and $d^X_{\max}(Y)$, where $d^X_{\max}(Y)$ is set to the first-dip position in partial RDF between *X* and *Y* while $d^X_{\min}(Y)$ corresponds to a point where the partial RDF reaches 0.01 (see Fig. 1). By symmetry, $d^X_{\min(\max)}(Y) = d^Y_{\min(\max)}(X)$.

With the determined bonding ranges, one can obtain the probability of atom type *Y* of bonded neighbors, $P^X_{\text{type}}(Y)$, and that of coordination number (CN), $P^X_{\text{CN}}(N)$, around a certain type *X*. The results for *a*-GeSe are shown in Fig. 2. Obviously, $\sum_Y P^X_{\text{type}}(Y) = \sum_N P^X_{\text{CN}}(N) = 1$ for every *X*.

2.2. Generation of amorphous structures

With $d^X_{\min(\max)}(Y)$, $P^X_{\text{type}}(Y)$, and $P^X_{\text{CN}}(N)$ extracted from the reference configurations, we proceed on how to distribute atoms in a way that is consistent with these input parameters. The procedure is somewhat involved, and for the easy understanding, the flow chart of the schematic procedure is presented in Fig. 3. Broadly speaking, the present method consists of two steps in seed-and-coordinate style. In the first step (the upper box in Fig. 3), a "seed" atom (indexed with *i*) is introduced into the simulation box or it is simply selected if already exists in the box. Then, the seed atom is coordinated with other atoms (indexed with *j*) in a way consistent with the input parameters. This second step corresponds to the "coordination" mode (the lower box in Fig. 3). In the below, we provide further details for each step.

(i) *Seeding step:* if *i* = *j*, this atom is not in the simulation box and should be first put inside the box. This new seed atom is assigned the atom type $\alpha(i)$ that is randomly chosen within the given stoichiometry. The CN of this atom ($CN_0(i)$) is selected on the basis of $P^{\alpha(i)}_{\text{CN}}$ in a probabilistic way. Then, this *i*th atom is put at a random position $\mathbf{R}(i)$ that is sufficiently away from the other atoms present in the box,

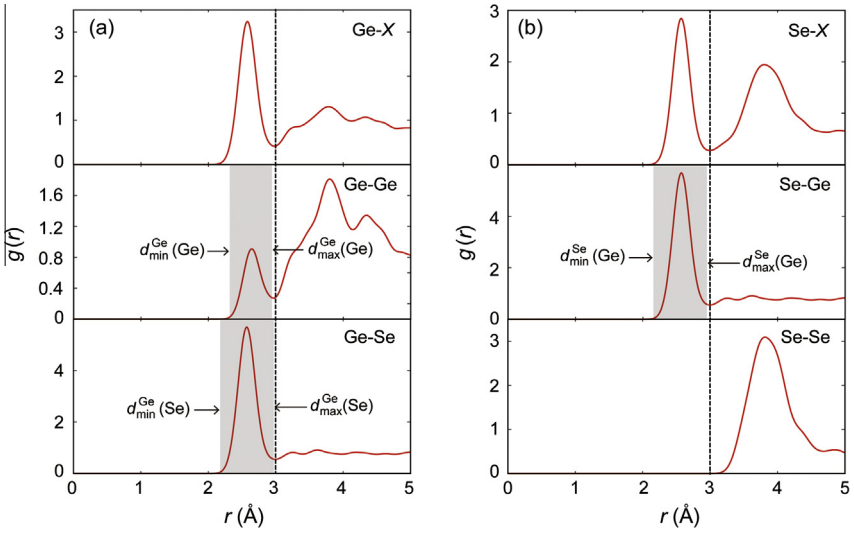

Fig. 1. The atom-resolved radial distribution function, $g(r)$, of (a) Ge and (b) Se in *a*-GeSe. The dashed line and shaded areas indicate the cutoff distance for defining the atomic bond and the ranges of the bond lengths between atom types, respectively.

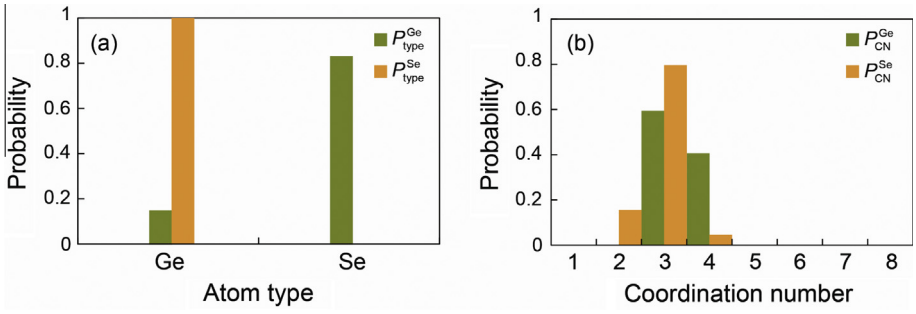

Fig. 2. Probability of (a) atom types and (b) coordination numbers around Ge and Se in *a*-GeSe.

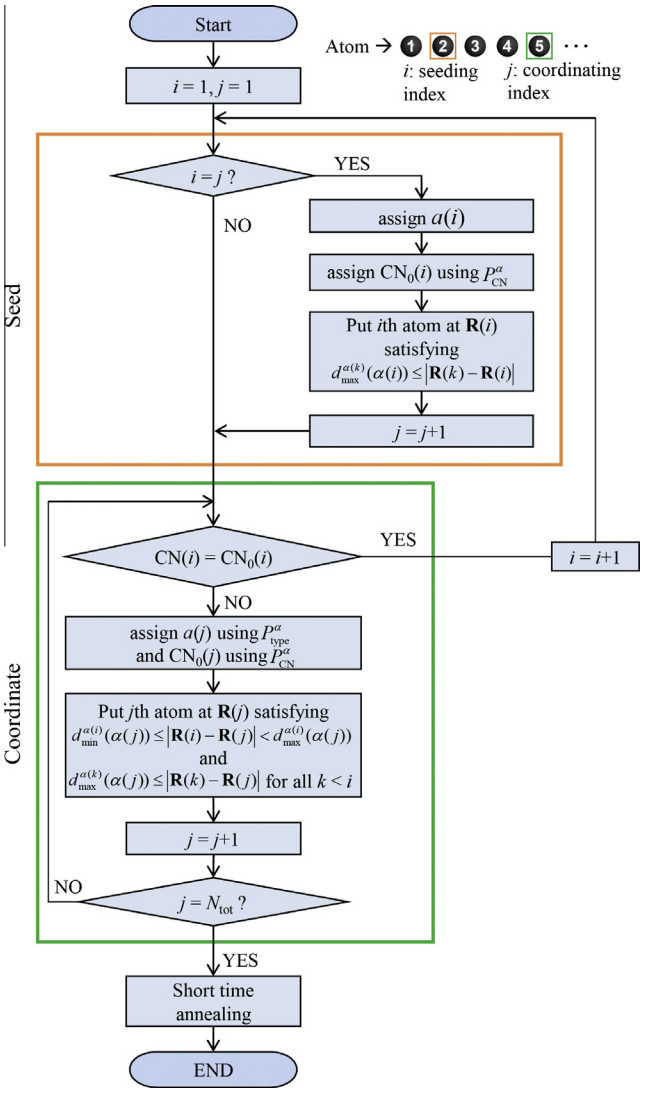

Fig. 3. Algorithm of seed-coordinate-anneal (SCA) method.

such that no additional bonds accompany the insertion of the *i*th atom. (Specifically, $d_{\max}^{\alpha(k)}(\alpha(i)) \leqslant |\mathbf{R}(k) - \mathbf{R}(i)|$ for every atom *k* in the box.) If $i \neq j$, this means that the seed atom is already in the box, so one needs only to coordinate it in the next step.

(ii) *Coordinating step:* it is first checked whether the present CN(i) is equal to the target value, $CN_0(i)$. If not, this means that additional bonds should be formed around *i*th atom. (Note that CN(i) is always less than or equal to $CN_0(i)$ according to the algorithm.) The index *j* for the coordinating atom is then incremented and the new neighboring atom is introduced into the box after the atom type and coordination number are assigned as $\alpha(j)$ and $CN_0(j)$, respectively. These two parameters are generated on the basis of $P_{\text{type}}^{\alpha(i)}$ and $P_{\text{CN}}^{\alpha(j)}$, respectively. Then the *j*th atom is put at $\mathbf{R}(j)$ around *i*th atom such that $d_{\min}^{\alpha(i)}(\alpha(j)) \leqslant |\mathbf{R}(i) - \mathbf{R}(j)| < d_{\max}^{\alpha(i)}(\alpha(j))$ and $d_{\max}^{\alpha(k)}(\alpha(j)) \leqslant |\mathbf{R}(k) - \mathbf{R}(j)|$ for all $k < i$ are satisfied. The former condition ensures that the neighboring atom is in bond with the seed atom, while the latter condition prevents the new atom from forming additional bond with the atoms that are already fully coordinated.

The above two steps are repeated until all atoms are configured inside the box.

Through the above procedure, the primary amorphous structure can be obtained. Further relaxation is required because of two reasons: first, we did not consider the angle distribution within the first shell. Second, any existing medium-range order is missed in the above procedure. To make up these deficiencies and improve the quality of amorphous structures, we carry out a short-time MD simulation below the melting temperature (annealing step). In the following, we call the whole procedure "seed-coordinate-anneal" (SCA) method.

3. Results and discussions

3.1. Computational setup

Using the SCA method outlined in the previous section, we generate amorphous structures for various materials encompassing *a*-Si, *a*-SiO_2, *a*-$Ge_2Sb_2Te_5$ (*a*-GST), and *a*-$InGaZnO_4$ (*a*-IGZO), that are widely used in various applications. We employ the DFT-based code, Vienna *ab initio* simulation package (VASP) [38] for all the computations in this work. The ion–electron interactions are approximated by the pseudopotentials of the projector-augmented wave (PAW) type [39]. The generalized gradient approximation (GGA) [40] is used for the exchange-correlation energy between electrons. The energy cutoff for a plane-wave basis is chosen to be 500 eV for every material and the **k**-point is sampled only at the gamma point.

Table 1
The simulation parameters for MQ and SCA methods. The cooling rate in MQ is applied until the temperature is lowered to 300 K.

Methods	Parameter	*a*-Si	*a*-SiO_2	*a*-GST	*a*-IGZO
MQ	Melting temperature (K)	2500	3000	1000	2500
	Melting time (ps)	20	20	30	20
	Cooling rate (K/ps)	250	250	60	250
SCA	Annealing temperature (K)	1500	2200	500	1500

To obtain the input parameters for the SCA method, the reference amorphous structure is generated for each material through the standard MQ procedure (see Table 1). Since the SCA method requires the information on the atomic bonding within the first shell, relatively small numbers of atoms (64, 96, 72, and 112 atoms for *a*-Si, *a*-SiO_2, *a*-GST, and *a*-IGZO, respectively) are included at this stage. Then, the amorphous structures with larger numbers of atoms are built according to the SCA method. Specifically, 144, 144, and 216 atoms are employed for *a*-Si, *a*-SiO_2, and *a*-GST, respectively. (In the case of *a*-IGZO, the 112-atom cell is already enough for characterizing up to the medium-range order and so the supercell size is not increased.) These SCA structures are then verified by comparison with the same-size MQ structures with the same temperature protocol as above. The annealing temperatures used in the SCA methods are also provided in Table 1. Regarding the annealing time, we find that 4 ps is enough for all the materials. In the below, we compare structural and electronic properties between MQ and SCA structures.

3.2. Structural properties

Fig. 4 compares the total RDF of each amorphous material obtained by SCA and MQ methods. The good agreements are found for all the materials. In particular, it is noticeable that the RDFs beyond the first shell are also similar even though only the information of the first-nearest neighbor was used for generating the SCA structure. We note that the structure after the seed-coordinate step deviate significantly from the distribution in Fig. 4, which means that the annealing step is essential in refining the short-range order and establishing the medium- or long-range orders.

The average CNs are also similar between the two methods. For instance, the MQ and SCA methods result in the average CNs of 4 and 2 for Si and O in *a*-SiO_2, respectively. For *a*-IGZO, the results of the SCA method (In: 5.8, Ga: 5.2, Zn: 4.7, and O: 3.9) are also in good agreement with MQ values (In: 5.9, Ga: 5.0, Zn: 4.7, and O: 3.9). The detailed distributions of CNs are shown in Table 2 for *a*-Si and *a*-GST. The structural defect of 3- or 5-fold coordinated Si atoms in *a*-Si are found both for MQ and SCA results [41,42]. It is known that the mixed bonding character in *a*-GST leads to a complicated local order of Ge [43,44]. As a result, the CNs in *a*-GST are distributed more widely than other amorphous materials. Such an intricate bonding nature is also revealed in the SCA structure and the overall distribution of the CNs agrees well with the MQ results. In addition, we examine in Fig. 5 the ring structures in *a*-GST because they are critical to the amorphous stability and the crystallization speed [45,46]. It is seen that the

Table 2
The fraction (in %) of atoms with certain coordination numbers in *a*-Si and *a*-GST.

			Coordination number					
			1	2	3	4	5	6
a-Si	Si	SCA	0.00	0.00	1.39	95.83	2.78	0.00
		MQ	0.00	0.00	0.00	94.44	5.56	0.00
a-GST	Ge	SCA	0.00	0.00	37.50	54.17	4.17	4.17
		MQ	0.00	0.00	43.75	50.00	4.17	2.08
	Sb	SCA	0.00	2.08	70.83	22.92	4.17	0.00
		MQ	0.00	0.00	66.67	31.25	2.08	0.00
	Te	SCA	0.00	46.67	51.67	1.67	0.00	0.00
		MQ	0.83	44.17	50.83	4.17	0.00	0.00

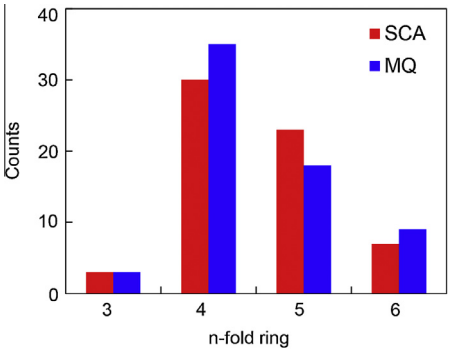

Fig. 5. Ring distributions in *a*-GST counted per supercell.

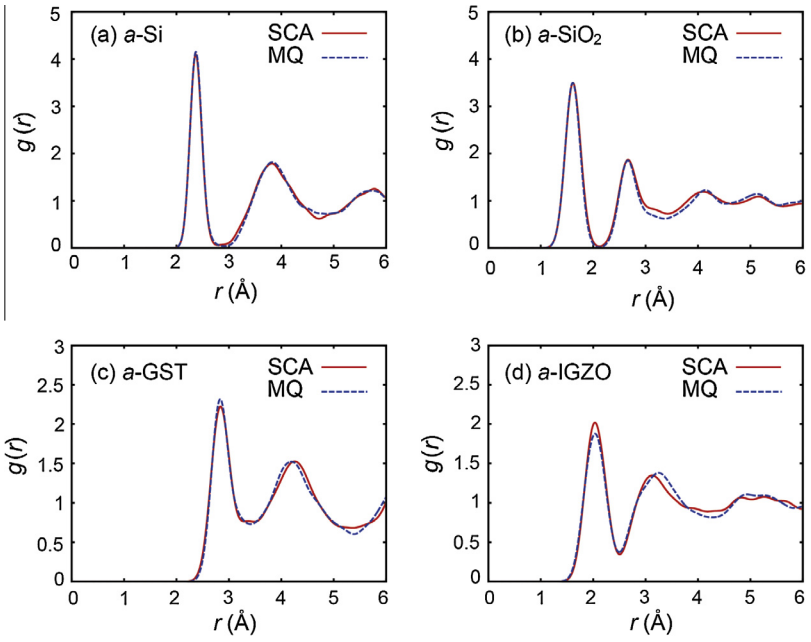

Fig. 4. The comparison of the total radial distribution functions, $g(r)$, in SCA and MQ structures. (a) *a*-Si, (b) *a*-SiO_2, (c) *a*-GST, and (d) *a*-IGZO.

Table 3
The energy and density ratio of the amorphous materials with respect to the crystalline counterparts (diamond Si, α-quartz SiO_2, cubic GST, and rhombohedral IGZO).

		a-Si	*a*-SiO_2	*a*-GST	*a*-IGZO
Energy (meV/atom)	SCA	268	125	110	156
	MQ	245	81	93	159
Density ratio	SCA	0.99	0.82	0.93	0.97
	MQ	1.01	0.82	0.93	0.98
	Exp.	0.98[a]	0.83[b]	0.94[c]	0.96[d]

[a] Ref. [47].
[b] Ref. [48].
[c] Ref. [49].
[d] Ref. [50].

overall agreement is reasonable and both results show consistently that the 4-fold rings dominate the distribution.

3.3. Energy and density

Next, we examine the energy and density of the amorphous structures. In Table 3, the energies of the amorphous structures relative to the crystalline values are shown. It is found that the MQ and SCA energies show good agreements within 20 meV/atom except for *a*-SiO_2 in which the SCA structure is less stable than the MQ one by ~40 meV/atom. The analysis on the atomic structure reveals that this is due to the presence of a pair of 3- and 5-fold Si atoms in the SCA structure in contrast to the MQ structure where all Si atoms satisfy 4-fold tetrahedral bonding. This pair of miscoordinated Si atoms was removed by the additional MD simulation at 3000 K for 2 ps, and the energy is lowered to within 10 meV/atom of the MQ value.

The density of the amorphous structure is usually decreased in comparison with the crystalline phase due to the loose atomic packing. This is confirmed in the present simulations using both MQ and SCA methods as shown in Table 3. The agreement between theories and experiment is reasonable. For *a*-Si, the density of amorphous phase is slightly larger in MQ than the crystalline value, but this due to the statistical fluctuation; we find that the ratio is reduced to 0.99 when averaged over several MQ structures.

3.4. Electronic structures

Finally, we compare electronic structures between SCA and MQ methods. Due to the aperiodicity in the amorphous phase, the band structure is not well defined and the density of states (DOS) is the main quantity that determines the electrical property of amorphous materials. In addition, the localization of the wave function is also important because it provides the information on the mobility edge that separates the localized and delocalized (conducting) states near the Fermi level. The degree of localization can be quantified by the inverse participation ratio (IPR) [51] defined as follows:

$$\mathrm{IPR} = \frac{\sum_i |a_i|^4}{\left(\sum_i |a_i|^2\right)^2}, \tag{1}$$

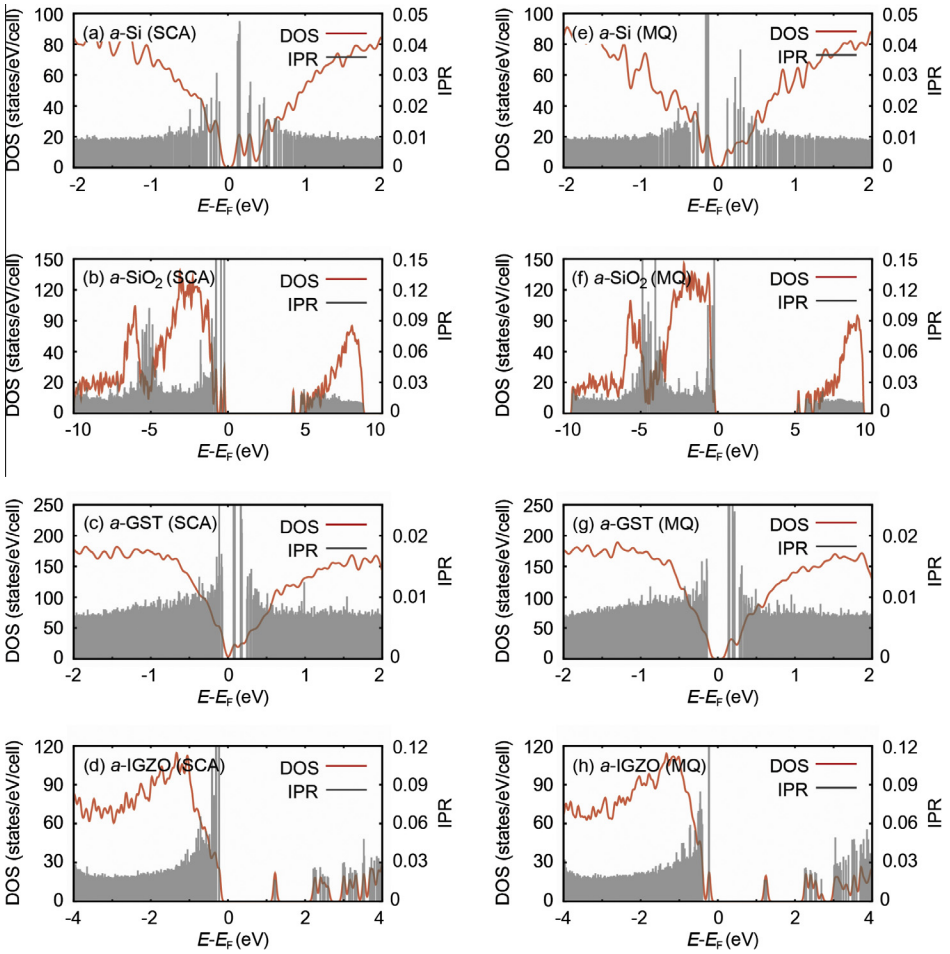

Fig. 6. Comparison of DOS and IPR near the Fermi level (E_F) between SCA and MQ results.

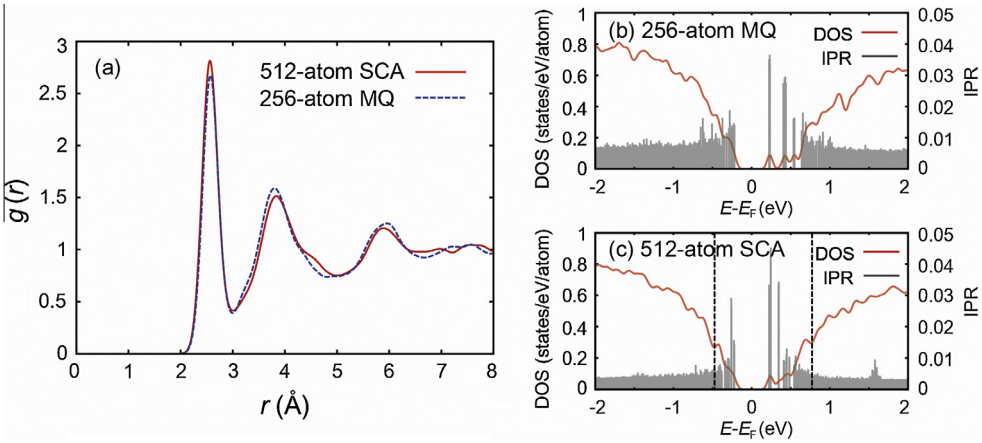

Fig. 7. (a) Total radial distribution functions of *a*-GeSe. The DOS and IPR near the Fermi level (E_F) of *a*-GeSe with (b) 256 and (c) 512 atoms. Dashed lines in (c) show the approximate position of the mobility edge.

where $|a_i|$ is the partial weight on the ith atom. For example, if a specific state is equally distributed over the N atoms, IPR is equal to $1/N$. The computed DOS and IPR are displayed in Fig. 6 for all the tested materials. It is found that the magnitude of the fundamental gap and the distribution of IPR profile near the Fermi level agree reasonably between MQ and SCA methods.

In the case of *a*-IGZO, the characteristic coupling between metal-*s* and oxygen-*p* orbitals in the unoccupied levels leads to the crystalline dispersion relation even in the amorphous structure. [52] This means that one can define the effective mass (m^*) for the conduction band in *a*-IGZO. This can be obtained from energy (ε) versus k relation as follows:

$$m^* = \hbar^2 \cdot \left[\frac{d^2\varepsilon}{dk^2}\right]^{-1}, \quad (2)$$

where $\hbar$ is the Planck constant. We fit the band near the gamma point and the effective masses are computed to be 0.173 and 0.166 m_0 for the SCA and MQ structures, respectively, which again confirms that the electronic structures in the two methods are similar.

3.5. *a*-GeSe in large cell

The computational advantage of the SCA method is manifest when generating a large model of the amorphous structure including, for example more than 500 atoms, which would take months of computational time within the MQ approach. It was reported that some important electronic properties of the amorphous materials, for example the mobility edge, are not clearly observed in a small supercell [53,54]. To demonstrate the usefulness of the present method and also to examine the influence of the supercell size on the electronic structures of the amorphous materials, we made two structures of *a*-GeSe with 256 and 512 atoms by applying the MQ and SCA methods, respectively. (It took us about one week to generate 512-atom model using 256 cores of Intel Xeon X5570 Nehalem 2.93 GHz.) It is seen that the atomic structures show good agreement as shown in Fig. 7(a), but the electronic structures in Fig. 7(b) and (c) are slightly different. In particular, the distribution of IPR is much smoother in 512-atom structure, and the separation between delocalized and localized states near the band edge (especially, the valence band edge) is more evident in the 512-atom supercell in comparison with 256-atom supercell. The mobility edge can be estimated by the decaying profile of the IPR values as the energy shifts away from the Fermi level. Fig. 7(c) shows that it is ~0.25 (0.55) eV lower (higher) than the edge of occupied (unoccupied) states. Experimentally, it was reported that the total width of the localized states is ~0.7 eV [55] which agrees well with ~0.8 eV from the present calculation.

4. Summary and conclusion

In summary, we proposed an efficient scheme dubbed as the SCA method that generates the amorphous structure. It consists of (i) seed-and-coordinate step to quickly make the base amorphous structure that is consistent with the given short-range order and (ii) short time annealing to refine the amorphous structures. The proposed method was more than 10 times faster than DFT-based MQ methods. Test calculations were performed on various types of amorphous materials encompassing *a*-Si, *a*-SiO_2, *a*-$Ge_2Sb_2Te_5$ and *a*-$InGaZnO_4$, and the reliability and accuracy of the SCA method were thoroughly verified by comparing RDF, energy, density, DOS, and IPR with the reference MQ data. The usefulness of the SCA method was demonstrated by 512-atom *a*-GeSe model in which we were able to locate the mobility edge to a good precision. We believe that the SCA method can be widely used in generating amorphous structures on a large scale or multiple times for the statistical average. The program will be available at http://mtcg.snu.ac.kr.

Acknowledgements

This work was supported by the Fundamental R&D Program for Core Technology of Materials. The computations were carried out at the KISTI Supercomputing Center (KSC-2013-C3-039).

References

[1] P.G. LeComber, W.E. Spear, A. Ghaith, Electron. Lett. 15 (1979) 179.
[2] M.J. Powell, IEEE Trans. Electron Devices 36 (1989) 2753.
[3] K. Nomura, H. Ohta, A. Takagi, T. Kamiya, M. Hirano, H. Hosono, Nature 432 (2004) 488.
[4] H. Hosono, J. Non-Cryst. Solids 352 (2006) 851.
[5] Y. Kang, Y. Cho, S. Han, Appl. Phys. Lett. 102 (2013) 152104.
[6] H.Y. Jung, Y. Kang, A.Y. Hwang, C.K. Lee, B.G. Son, C.-K. Lee, H.J. Kim, S. Han, D.-H. Kim, J.-U. Bae, W.-S. Shin, J.K. Jeong, Sci. Rep. 4 (2014) 3765.
[7] Y. Jiao, X. Zhang, J. Zhai, X. Yu, L. Ding, W. Zhang, Electron. Mater. Lett. 9 (2013) 279.
[8] C.-S. Yang, L.L. Smith, C.B. Arthur, G.B. Parsons, J. Vac. Sci. Technol. B 18 (2000) 683.
[9] A.L. Lacaita, D.J. Wouters, Phys. Status Solidi A 205 (2008) 2281.
[10] M.H.R. Lankhorst, B.W. Ketelaars, R.A.M. Wolters, Nat. Mater. 4 (2005) 347.
[11] B.-k. Cheong, S. Lee, J.-h. Jeong, S. Park, S. Han, Z. Wu, D.-H. Ahn, Phys. Status Solidi B 249 (2012) 1985.
[12] D.S. Jeong, H.-W. Ahn, S.-D. Kim, M. An, S. Lee, Electron. Mater. Lett. 8 (2012) 169.

[13] D.A. Drabold, Eur. Phys. J. B 68 (2009) 1.
[14] A. Hannemann, J.C. Schön, M. Jansen, H. Putz, T. Lengauer, Phys. Rev. B 70 (2004) 144201.
[15] F. Wooten, K. Winer, D. Weaire, Phys. Rev. Lett. 54 (1985) 1392.
[16] M.M.J. Treacy, J.M. Gibson, Acta Crystallogr. A52 (1996) 212.
[17] G.T. Barkema, N. Mousseau, Phys. Rev. Lett. 77 (1996) 4358.
[18] N. Mousseau, L.J. Lewis, Phys. Rev. Lett. 78 (1997) 1484.
[19] D. Vanderbilt, X. Zhao, D. Ceresoli, Thin Solid Films 486 (2005) 125.
[20] G.T. Barkema, N. Mousseau, Comput. Mater. Sci. 20 (2001) 285.
[21] J. Tersoff, Phys. Rev. Lett. 61 (1998) 2879.
[22] F. De Brito Mota, J.F. Justo, A. Fazzio, Phys. Rev. B 58 (1998) 8323.
[23] A.Yu. Belov, Comput. Mater. Sci. 27 (2003) 30.
[24] M.V.R. Murty, H.A. Atwater, Phys. Rev. B 51 (1995) 4889.
[25] R. Car, M. Parrinello, Phys. Rev. Lett. 60 (1988) 204.
[26] J. Sarnthein, A. Pasquarello, R. Car, Phys. Rev. Lett. 74 (1995) 4682.
[27] J. Hegedüs, S.R. Elliott, Nat. Mater. 7 (2008) 399.
[28] D.G. McCulloch, D.R. McKenzie, C.M. Goringe, Phys. Rev. B 61 (2000) 2349.
[29] S. Le Roux, A. Bouzid, M. Boero, C. Massobrio, Phys. Rev. B 86 (2012) 224201.
[30] F. Finocchi, G. Galli, M. Parrinello, C.M. Bertoni, Phys. Rev. Lett. 68 (1992) 3044.
[31] J.A. Reyes-Retana, A.A. Valladares, Comput. Mater. Sci. 47 (2010) 934.
[32] X. Zhao, D. Ceresoli, D. Vanderbilt, Phys. Rev. B 71 (2005) 085107.
[33] N.C. Cooper, C.M. Goringe, D.R. Mckenzie, Comput. Mater. Sci. 17 (2000) 1.
[34] J. Akola, R.O. Jones, Phys. Rev. B 76 (2007) 235201.
[35] Y. Kang, H. Song, H.-H. Nahm, S.H. Jeon, Y. Cho, S. Han, APL Mater. 2 (2014) 032108.
[36] S. Kohara, K. Kato, S. Kimure, H. Tanaka, T. Usuki, K. Suzuya, H. Tanaka, Y. Moritomo, T. Matsunaga, N. Yamada, Y. Tanaka, H. Suematsu, M. Takata, Appl. Phys. Lett. 89 (2006) 201910.
[37] S. Kugler, L. Pusztai, L. Rosta, P. Chieux, R. Bellissent, Phys. Rev. B 48 (1993) 7685.
[38] G. Kresse, J. Furthmuller, Phys. Rev. B 54 (1996) 11169.
[39] P.E. Blöchl, Phys. Rev. B 50 (1994) 17953.
[40] J.P. Perdew, K. Burke, M. Ernzerhof, Phys. Rev. Lett. 77 (1996) 3865.
[41] I. Štich, R. Car, M. Parrinello, Phys. Rev. B 44 (1991) 11092.
[42] J. Fortner, J.S. Lannin, Phys. Rev. B 39 (1989) 5527.
[43] S. Caravati, M. Bernasconi, T.D. Kühne, M. Krack, M. Parrinello, Appl. Phys. Lett. 91 (2007) 171906.
[44] K.Y. Kim, J. Appl. Phys. 113 (2013) 134302.
[45] J. Im, E. Cho, D. Kim, H. Horri, J. Ihm, S. Han, Phys. Rev. B 81 (2010) 245211.
[46] E. Cho, Y. Youn, S. Han, Appl. Phys. Lett. 99 (2011) 183501.
[47] J.S. Custer, M.O. Thompson, D.C. Jacobson, J.M. Poate, S. Roorda, W.C. Sinke, Appl. Phys. Lett. 64 (1994) 437.
[48] S.R. Elliott, Physics of Amorphous Materials, second ed., Wiley, New York, 1990.
[49] W. Njoroge, H.-W. Wöltegens, M. Wuttig, J. Vac. Sci. Technol. A 20 (2002) 230.
[50] T. Kamiya, K. Nomura, H. Hosono, J. Display Technol. 5 (2009) 273.
[51] F. Wegner, Z. Phys. B 36 (1980) 209.
[52] Y. Kang, S.H. Jeon, Y.-W. Son, Y.-S. Lee, M. Ryu, S. Lee, S. Han, Phys. Rev. Lett. 108 (2012) 196404.
[53] J. Seo, H.-W. Ahn, Appl. Phys. Lett. 104 (2014) 153503.
[54] J. Dong, D.A. Drablod, Phys. Rev. Lett. 80 (1998) 1928.
[55] T.T. Nang, M. Okuda, T. Matsushita, S. Yokota, A. Suzuki, Jpn. J. Appl. Phys. 15 (1976) 849.